Computational Materials Science 258 (2025) 114087

Contents lists available at ScienceDirect

Computational Materials Science

journal homepage: www.elsevier.com/locate/commatsci

Full length article

Mechanical strength and strain-induced optical shifts in monolayer azugraphene

Mizraim Bessa [a], Dênis G. de Medeiros Dantas [a], Djardiel da Silva Gomes [b,c], Marcelo L. Pereira Jr. [d,e], Sérgio Azevedo [a,b], Leonardo D. Machado [a,*]

[a] Departamento de Física, Universidade Federal do Rio Grande do Norte, 59078-900, Natal, RN, Brazil
[b] Departamento de Física, Universidade Federal da Paraíba, 58050-585, João Pessoa, PB, Brazil
[c] Universidade Estadual de Campinas, Instituto de Física Gleb Wataghin, Departamento de Física Aplicada, Campinas, São, Paulo, 13083-859, Brazil
[d] University of Brasília, College of Technology, Department of Electrical Engineering, 70910-900, Brasília, DF, Brazil
[e] Materials Science and NanoEngineering Department, Rice University, 77005, Houston, TX, United States

ARTICLE INFO

Keywords:
Mechanical properties
Strain engineering
Optical Properties
Two-dimensional materials
Density Functional Theory

ABSTRACT

Azugraphene is a carbon allotrope with remarkably low energy per atom, predicted in 2019. Despite this, its mechanical properties and strain-dependent behavior remain largely unexplored. In this work, we perform first-principles calculations to investigate the mechanical, electronic, and optical properties of azugraphene under uniaxial strain. Our results show that azugraphene exhibits stiffness and strength comparable to graphene, with an isotropic mechanical response for small deformations. They also reveal that azugraphene evolves from a zero-gap semiconductor to a metallic state under high tensile deformation. Azugraphene also exhibits high reflectivity in the infrared and optical absorption peaks in the visible and ultraviolet ranges, which shift to lower energies in proportion to the applied tensile strain. Conversely, compressive strain shifts the absorption peaks to higher energies. The possibility of applying strain to tune the position of the visible light absorption peaks suggests azugraphene applications in optical sensors and solar cells.

1. Introduction

Studying two-dimensional (2D) materials has established itself as a relevant area within materials science, driven by the distinctive properties observed in systems such as graphene [1,2]. In this context, several 2D carbon allotropes based on sp^2 bonding have been continuously proposed, aiming to expand these materials' structural and functional diversity for potential applications in electronics, optoelectronics, and sensing devices [3]. Among these proposals is azugraphene, a carbon allotrope whose structural unit combines fragments of azulene molecules, hexagonal rings, and additional carbon atoms [4]. This results in a planar network of pentagons, heptagons, and hexagons.

Azugraphene was predicted in 2019 through a first-principles symmetric search algorithm, exhibiting a remarkably low energy per atom, only 157 meV above that of graphene [4]. Its structure, illustrated in Fig. 1(a), can be decomposed into three azulene units, one isolated hexagonal ring, and two additional atoms. Subsequent studies demonstrated that inserting azulene units into the hexagonal graphene lattice enables the formation of various stable structures [5]. Interest in azulene arises from its peculiar optoelectronic properties, such as the presence of an electron-rich pentagon and an electron-deficient heptagon, resulting in a notable electric dipole moment of 1.08 D, among other relevant characteristics [6–8]. These properties have motivated growing research efforts on azulene-based carbon allotropes, among which azugraphene is included [5].

Fig. 1(b) shows the rectangular unit cell of azugraphene, composed of 76 atoms. The classification scheme proposed by Girão et al. for two-dimensional sp^2-bonded carbon allotropes is adopted to characterize its structure [9]. Within this framework, azugraphene is designated as $h5^36^{13}7^3$-graphene, where the initial letter denotes the hexagonal symmetry and the numbers indicate the quantity of five-, six-, and seven-membered rings in the primitive cell. In its ground state, azugraphene exhibits a planar configuration with sp^2 hybridization and ranks among the most stable sp^2 carbon allotropes predicted to date [9]. However, its mechanical properties remain largely unexplored, and no systematic studies have been conducted regarding the effects of strain on its structural, electronic, and optical properties.

Several studies have shown that controlled mechanical deformation can significantly alter two-dimensional materials' electronic, magnetic,

* Corresponding author.
E-mail address: leonardo@fisica.ufrn.br (L.D. Machado).

https://doi.org/10.1016/j.commatsci.2025.114087
Received 1 May 2025; Received in revised form 16 June 2025; Accepted 29 June 2025
Available online 12 July 2025

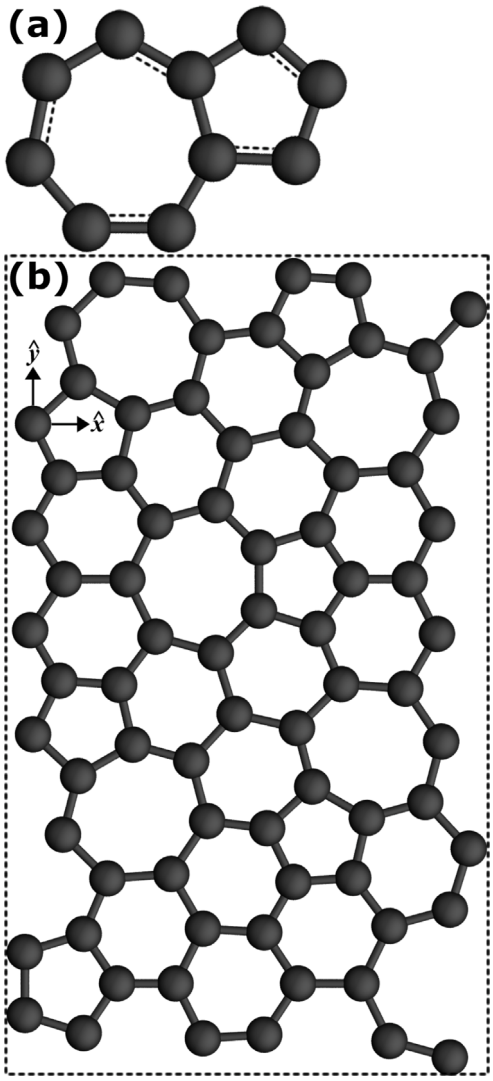

Fig. 1. (a) Azulene molecule, with dashed black lines representing π bonds and hydrogen atoms omitted. (b) Azugraphene unit cell considered in this work.

and optical properties [10–15]. The technique of modulating material properties through deformation, known as strain engineering, has been extensively applied, particularly in graphene studies [16–20]. For instance, previous research indicates that the application of strains greater than 20% can induce the opening of a significant bandgap in graphene [16,19,21]. Furthermore, strain-induced modifications can enhance the applicability of 2D carbon materials, such as azugraphene, in sensing [22–25] and wearable device applications [26–30].

In this work, we perform first-principles calculations to characterize previously unexplored properties of monolayer azugraphene, including its mechanical properties and the influence of strain on its structural, electronic, and optical behavior.

2. Computational methodology

An initial azugraphene structure, corresponding to its primitive cell and composed of 38 atoms, was obtained from the electronic supplementary material of J. Liu and H. Lu [4]. This structure was subsequently extended to generate a rectangular unit cell, allowing the consideration of two orthogonal directions for strain application. The final structure, shown in Fig. 1(b), contains 76 atoms per unit cell.

Density Functional Theory (DFT) calculations were performed to determine the mechanical properties of azugraphene and to investigate its electronic and optical properties under strain. Simulations were carried out using the Spanish Initiative for Electronic Simulations with Thousands of Atoms (SIESTA) code, employing the Perdew–Burke–Ernzerhof (PBE) functional [31] within the Generalized Gradient Approximation (GGA) framework to describe the exchange–correlation potential. The basis set consisted of finite-range pseudoatomic orbitals (PAO), described by a double-ζ basis set including polarization functions (DZP). Troullier–Martins norm-conserving pseudopotentials were used to model the electron–ion interactions. A real-space grid cutoff of 450 Ry was adopted for the charge density representation. All structures were fully optimized until the maximum residual atomic forces were below 0.01 eV/Å. The convergence criterion for the self-consistent field (SCF) cycle was set to 10^{-4} eV. Three-dimensional periodic boundary conditions (PBC) were applied, introducing a vacuum spacing of 30 Å along the $\hat{\mathbf{z}}$ direction to prevent interactions between periodic images. The Brillouin zone was sampled using a $16 \times 16 \times 1$ k-point mesh within the Monkhorst–Pack scheme [32].

We also performed calculations with the HSE06 hybrid functional within the HONPAS package [33] to verify whether the results depended on the exchange–correlation functional used. The hybrid functional results, which are discussed in the Supplementary Material, reveal that the PBE and HSE06 functionals yield similar electronic properties for azugraphene.

Initially, the azugraphene structure was optimized for a relaxed configuration (0% strain). Subsequently, uniaxial strain ranging from 1% to 20% was applied along the relaxed structure's x or y directions. The elongated cell vector was fixed for each strain value, while the other in-plane cell vector and the atomic positions were allowed to relax to new equilibrium configurations. After optimization, electronic and optical calculations were performed on the strained structures. The SIESTA code provided the stress values along the strained direction for each applied deformation.

The stress–strain curves for the x and y directions were obtained from the stress and strain data. By definition, Young's modulus $\boldsymbol{Y}$ corresponds to the slope of the linear regime of the stress–strain curve. To calculate $\boldsymbol{Y}$, the interval from 0 to 1% strain was subdivided into 0.1% increments, and a linear fit was applied. The coefficients of determination R^2 for both directions were also evaluated. The ultimate strength was defined as the maximum stress sustained by the material before fracture, while the fracture strain corresponded to the strain value at which the rupture occurred. Both parameters were extracted from the stress–strain curves. To convert stress results into pascals (Pa), a thickness of 3.4 Å was assumed for azugraphene, corresponding to the interlayer distance found in its stable bilayer configurations [4]. We also examine the dynamical stability of azugraphene under strain in the Supplementary Material. We note that, for the strain values considered, we observed only positive frequencies in the phonon spectra.

To examine the fracture patterns, we analyzed the electron density of azugraphene under various uniaxial strain values. The electron density we use is an output of the SIESTA code. More specifically, SIESTA provides the magnitude of the valence charge density in the real-space grid, with a fineness determined by the grid cutoff (450 Ry in this work). Next, we use a SIESTA utility (rho2sxf) to convert the electron density file into a format that can be read by the software XCrysDen [34], which is used to generate the electron density maps discussed in the Results and discussion section.

The energy was shifted for the band structure and density of states (DOS) calculations so that the Fermi level corresponded to $E = 0$. The k-path for band structure calculations followed the high-symmetry points $\mathbf{\Gamma}(0.0, 0.0, 0.0) \rightarrow \mathbf{X}(0.5, 0.0, 0.0) \rightarrow \mathbf{M}(0.5, 0.5, 0.0) \rightarrow \mathbf{Y}(0.0, 0.5, 0.0) \rightarrow \mathbf{\Gamma}$ within the rectangular unit cell's Brillouin zone.

To calculate the optical properties of azugraphene, the real and imaginary parts of the dielectric function $\epsilon(w)$ were computed using perturbation theory and the Kramers–Kronig relations [35–37]. Once

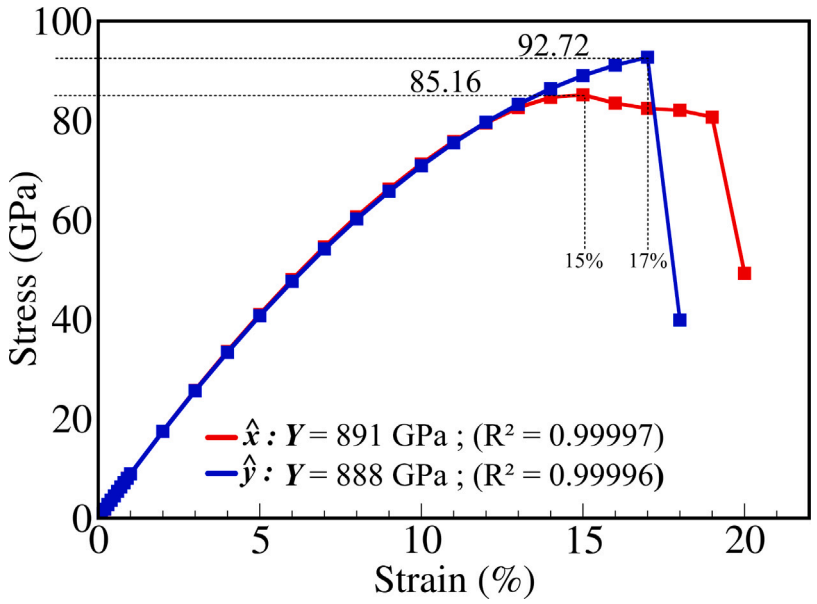

Fig. 2. Stress–strain curves for azugraphene under uniaxial strain. The $\hat{\mathbf{x}}$ ($\hat{\mathbf{y}}$) direction exhibits a slightly higher fracture strain (ultimate strength).

both components of the dielectric function were obtained, the optical properties were derived using the following relations [38–40]:

$$R(w) = \left| \frac{(\epsilon_R(w) + i\epsilon_I(w))^{1/2} - 1}{(\epsilon_R(w) + i\epsilon_I(w))^{1/2} + 1} \right|^2 \times 100\%, \tag{1}$$

$$\alpha(w) = \frac{2w}{c} \left[\frac{[\epsilon_R^2(w) + \epsilon_I^2(w)]^{1/2} - \epsilon_R(w)}{2} \right]^{1/2}, \tag{2}$$

and

$$\sigma(w) = \frac{w}{4\pi} \mathrm{Re} \left\{ \epsilon_I(w) - i \left[\epsilon_R(w) - 1 \right] \right\}, \tag{3}$$

where $R(w)$, $\alpha(w)$, and $\sigma(w)$ represent the reflectivity, absorption coefficient, and optical conductivity, respectively; $w = E/\hbar$ is the frequency of the incident photons, and c is the speed of light in vacuum.

3. Results and discussion

In this section, we first discuss the mechanical properties of azugraphene under uniaxial tensile strain. Fig. 2 presents the stress–strain curves obtained for both directions. Comparing the results along the $\hat{\mathbf{x}}$ and $\hat{\mathbf{y}}$ directions, it is observed that Young's modulus is nearly identical in both cases, with a slightly higher value along the $\hat{\mathbf{x}}$ direction. These results indicate that azugraphene exhibits comparable stiffness regardless of the deformation direction, with Young's modulus similar to that of graphene (which is 1.0 TPa [41]).

The similarity of Young's modulus values along the $\hat{\mathbf{x}}$ and $\hat{\mathbf{y}}$ directions was expected, considering the crystalline symmetry of azugraphene. In particular, the $P6\bar{2}m$ space group, associated with the hexagonal crystal system, implies that the structure remains invariant under rotations of 60° around the $\hat{\mathbf{z}}$ axis [4]. This high degree of basal plane symmetry favors the emergence of nearly isotropic mechanical properties for small deformations, particularly concerning Young's modulus.

For strain values exceeding 13%, anisotropy emerges in the mechanical response. Along the $\hat{\mathbf{x}}$ direction, azugraphene exhibits a lower ultimate strength (85.2 GPa) but a higher fracture strain (19%), indicating plastic behavior between 15% and 19% strain. In contrast, under deformation along the $\hat{\mathbf{y}}$ direction, the material shows a higher ultimate strength (92.7 GPa) and fractures abruptly at 17%, characterizing a more brittle behavior. This difference in post-critical behavior indicates that azugraphene can exhibit either ductile or brittle responses depending on the loading direction. The ultimate strength of azugraphene is also comparable to that of graphene, reported to be approximately 130 GPa [42].

Table 1
Summary of the mechanical properties of azugraphene under uniaxial strain.

Property	Direction	
	$\hat{x}$	$\hat{y}$
Young's Modulus (GPa)	891	888
Ultimate Strength (GPa)	85.2	92.7
Fracture Strain (%)	19	17

The quality of the linear fittings used to determine Young's modulus in both directions, with coefficients of determination R^2 greater than 0.9999, reinforces the validity of the linear approximation for small strains. Table 1 summarizes the mechanical properties of azugraphene.

To further investigate the mechanical response of azugraphene, we analyzed the fracture process of the nanomaterial. Fig. 3 presents the electronic density of the system's unit cell under different levels of uniaxial strain. Electronic density was used in this analysis to avoid the arbitrary definition of a distance criterion between atomic pairs to identify bond rupture. The image in the lower left corner displays the electronic density of the relaxed structure. It is observed that pentagonal rings exhibit higher electronic density compared to heptagonal rings, in agreement with previous reports [5]. A high electronic density between bonded atoms is also noted, characterizing the chemical bonds. In the methodology adopted, a significant reduction in electronic density between a pair of atoms is associated with dissociating a π bond. In contrast, an almost complete reduction is interpreted as a σ bond rupture.

An analysis of the structural evolution under strain along the $\hat{\mathbf{x}}$ direction reveals a gradual reduction in electronic density between hexagonal and heptagonal rings between 0% and 15% strain. As the strain increases to 18% and 19%, the rupture of these bonds becomes evident, subsequently propagating to neighboring bonds. The evolution of the electronic density suggests a progressive fracture process, characteristic of plastic behavior, consistent with the observations from the stress–strain curves.

In the case of deformation applied along the $\hat{\mathbf{y}}$ direction, a generalized reduction in electronic density is already observed between

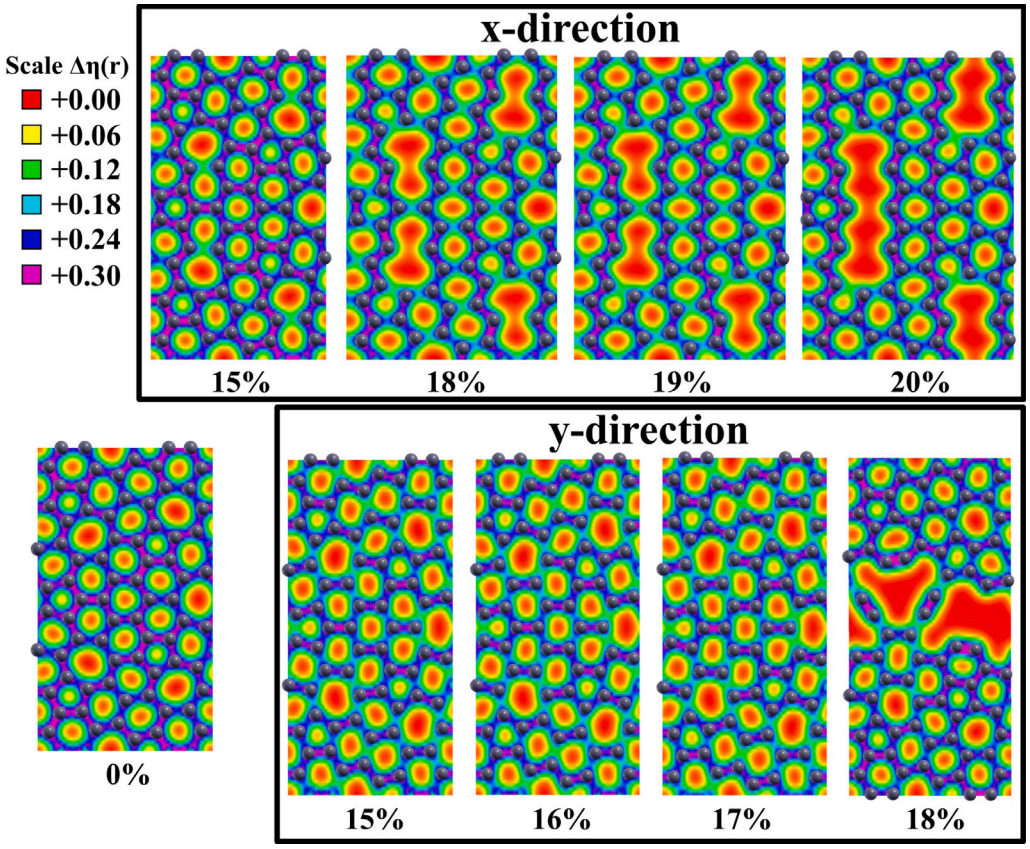

Fig. 3. Electronic density of azugraphene under different uniaxial strain values. The image in the lower left corner corresponds to the relaxed structure, while the sequences at the top (bottom) show the evolution of the electronic density under increasing strain along the $\hat{x}$ ($\hat{y}$) direction. The scale on the left indicates the density values of each color in arbitrary units.

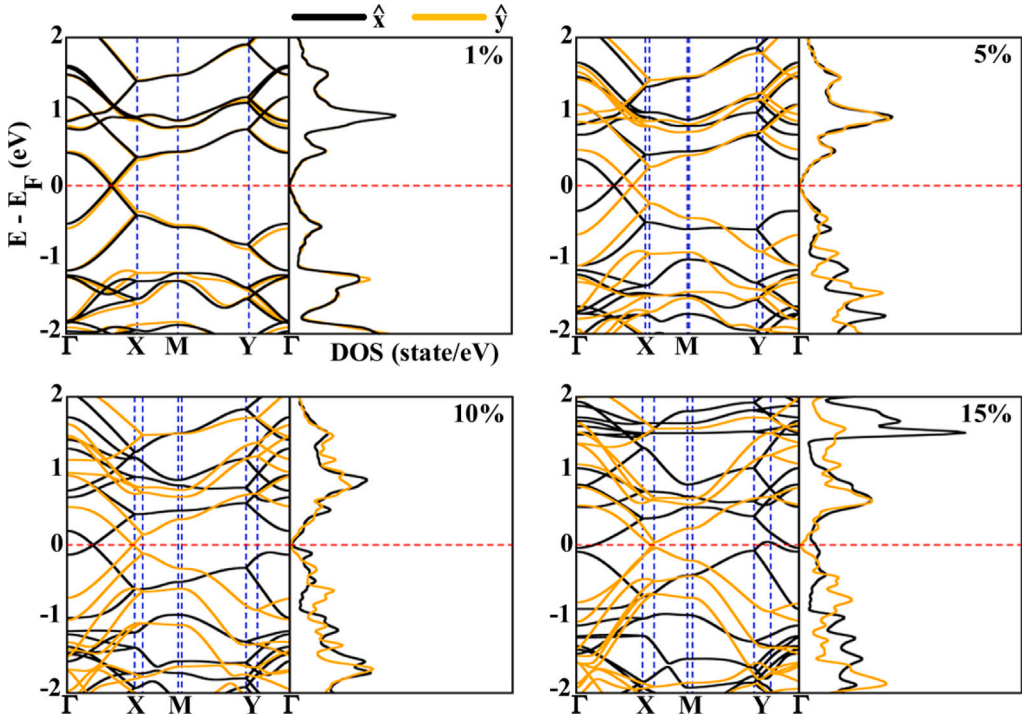

Fig. 4. Azugraphene's Band structure and DOS, for deformation values of 1%, 5%, 10%, and 15%.

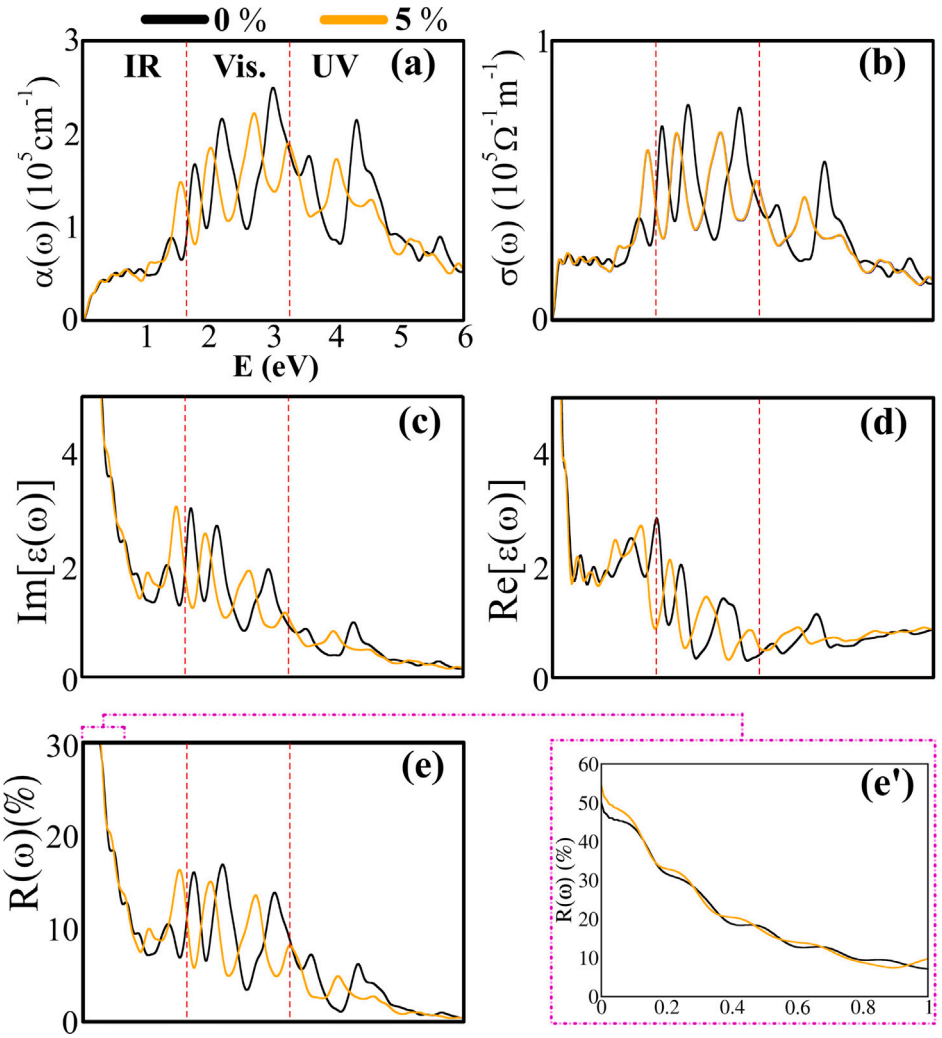

Fig. 5. Optical properties of azugraphene under 0% and 5% strain along the $\hat{\mathbf{x}}$ direction. Panels (a) and (b) show the absorption coefficient and optical conductivity. Panels (c) and (d) present the real and imaginary parts of the complex dielectric function. Panel (e) displays the reflectivity over the full energy range considered, while panel (e') focuses on the reflectivity at low photon energies (0–1 eV). The red dashed lines separate the infrared, visible, and ultraviolet regions.

15% and 17% strain across the structure. However, the complete rupture of σ bonds is only observed at 18%, when multiple fractures co-occur, particularly concentrated in the heptagonal rings and their surroundings. This behavior suggests an abrupt fracture process, typical of brittle materials, corroborating the tendency for brittle behavior of azugraphene under deformation along the $\hat{\mathbf{y}}$ direction.

Considering now the electronic properties, in the absence of strain, monolayer azugraphene is a zero-gap semiconductor featuring Dirac cones at the high symmetry K and K' points in the Brillouin zone [4]. Fig. 4 shows the band structure and density of states (DOS) of azugraphene under 1%, 5%, 10%, and 15% deformation. First, strain application does not open the band gap of azugraphene. For this reason, we leave a detailed discussion of the effect of strain on the electronic properties to the Supplementary Material, including the effect of compressive deformation on the electronic properties. In summary, we find that the introduction of strain displaces the position of the Dirac cones in the Brillouin zone. This effect is the only one we observe for strain applied in the $\hat{\mathbf{y}}$ direction.

Concerning deformation along the $\hat{\mathbf{x}}$ direction, we find that at 12% strain, azugraphene becomes metallic, exhibiting a significant density of states at the Fermi level. Overall, our results indicate that strain cannot be effectively used to tailor the electronic properties of azugraphene. Nevertheless, this electronic insensitivity could be advantageous for applications that require stable electronic properties under mechanical deformation.

Turning to the effect of strain on the optical properties, we focus our discussion on the case where strain is applied along the $\hat{\mathbf{x}}$ direction, as the results are more pronounced in this scenario. Figs. 5 and 6 compare the optical properties of azugraphene without strain and under 5% and 12% tensile strain for photon energies ranging from 0 to 6 eV. The red dashed lines indicate the infrared (IR), visible (Vis.), and ultraviolet (UV) regions of the electromagnetic spectrum.

Generally, azugraphene exhibits low absorption and high reflectivity in the IR region. The reflectivity at low photon energies (0–1 eV) can reach up to 55% (50%) for strains of 5% (12%), rapidly decreasing with increasing energy up to approximately 1 eV (see Figs. 5(e') and 6(e')), except for the 0.4–0.6 eV range under 12% strain, where a local increase in reflectivity is observed. Additionally, a comparison between Figs. 5(e') and 6(e') reveals that reflectivity at low energies decreases with increasing strain.

Moreover, under 12% strain, azugraphene exhibits three optical conductivity peaks in the IR region (Fig. 6(b)), which are absent at lower strain levels. These peaks suggest an enhancement of optical responses at low energies associated with the metallic transition observed in the material under high tensile strain.

In the Vis region of the spectrum, the relaxed structure exhibits three well-defined peaks in the absorption coefficient, optical conductivity, and reflectivity spectra. As the strain increases, the number of peaks in the Vis region decreases, leaving only a single peak at 12%

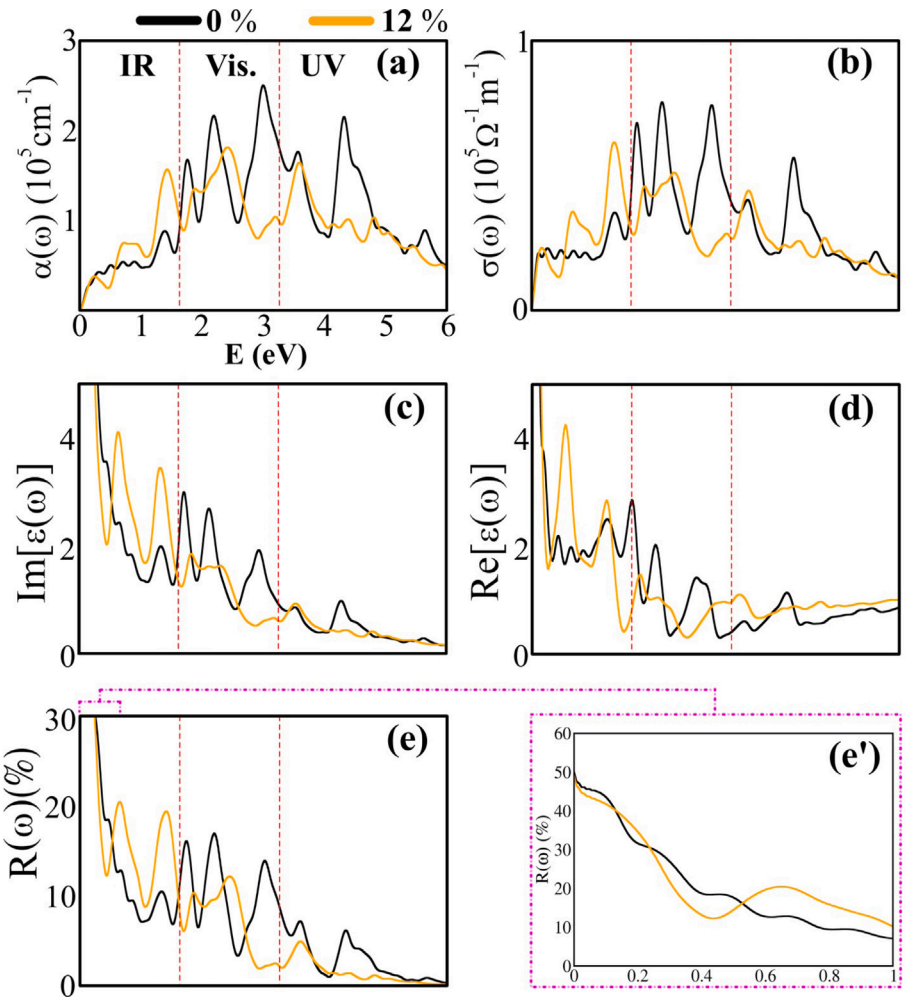

Fig. 6. Optical properties of azugraphene under 0% and 12% strain along the $\hat{\mathbf{x}}$ direction. Panels (a) and (b) show the absorption coefficient and optical conductivity. Panels (c) and (d) present the real and imaginary parts of the complex dielectric function. Panel (e) displays the reflectivity over the full energy range considered, while panel (e') focuses on the reflectivity at low photon energies (0–1 eV). The red dashed lines separate the infrared, visible, and ultraviolet regions.

strain. For instance, analyzing the blue and orange curves in Figs. 5(a) and 6(a), it is observed that the peaks in the Vis region undergo a shift to lower energies (redshift) and a reduction in intensity compared to the peaks of the relaxed structure.

For the other optical properties, increasing strain induces a proportional redshift, accompanied by a decrease in absorption, optical conductivity, and reflectivity in the Vis region. Conversely, this redshift favors increasing these properties within the IR region. We note that the Supplementary Material discusses the optical properties at additional strain levels.

Finally, a peak around 4.5 eV for the relaxed structure is observed in the UV region, progressively shifting towards the near-UV region with increasing strain. Therefore, we conclude that the optical properties of azugraphene can be modulated by applying strain. In particular, our results show that strain enhances the absorption, optical conductivity, and reflectivity in the IR region of the electromagnetic spectrum. Conversely, the magnitude of these properties decreases with increasing tensile strain in the Vis and UV regions. Moreover, tuning the position of the optical peaks is possible, as the redshift is proportional to the applied strain.

When strain is applied along the $\hat{\mathbf{y}}$ direction, the main effect is observed in the IR region, specifically within a photon energy range close to the Vis, where an increase in absorption, optical conductivity, and reflectivity is found at 12% strain. These results are discussed in greater detail in the Supplementary Material.

The effect of compressive strain on the optical properties is also discussed in the Supplementary Material. In summary, the results reveal that compressive strain tends to shift the peaks in the optical properties to higher photon energies (blueshift). Hence, it is possible to control the type (red or blue) and magnitude of the shifts in the peaks by selectively applying deformation.

4. Conclusions

In this work, we performed first-principles calculations to investigate the mechanical, electronic, and optical properties of monolayer azugraphene under strain. Our results demonstrate that azugraphene exhibits an isotropic mechanical response for tensile strains up to 13%, with Young's modulus comparable to that of graphene. Beyond this threshold, the mechanical behavior becomes anisotropic, with higher strength but lower fracture strain for deformation along the $\hat{\mathbf{y}}$ direction. Using electronic density analysis, we found that the fracture process initiates near the heptagonal rings, which is associated with the weakening of specific atomic bonds.

In terms of electronic properties, azugraphene behaves as a zero-gap semiconductor at equilibrium and evolves into a metallic state when subjected to tensile strains exceeding 12% along the $\hat{\mathbf{x}}$ direction.

Regarding optical properties, the relaxed structure exhibits well-defined absorption and optical conductivity peaks in the UV region, which progressively disappear under large tensile deformations along the $\hat{\mathbf{x}}$ direction. Additionally, azugraphene shows high reflectivity (approximately 55%) for low-energy IR photons, remaining relatively insensitive to strain. Furthermore, tensile strain induces a proportional redshift in the optical absorption, optical conductivity, and reflectivity spectra, suggesting that mechanical deformation can be used to tune the optical response of azugraphene. Conversely, a compressive strain shifts the optical response of this material to higher energies. These findings highlight the potential of azugraphene for applications in optical sensors and solar energy harvesting devices.

CRediT authorship contribution statement

Mizraim Bessa: Writing – original draft, Methodology, Investigation, Formal analysis. **Dênis G. de Medeiros Dantas:** Writing – review & editing, Validation, Investigation. **Djardiel da Silva Gomes:** Writing – review & editing, Methodology, Investigation. **Marcelo L. Pereira Jr.:** Writing – review & editing, Validation, Supervision. **Sérgio Azevedo:** Writing – review & editing, Validation, Methodology. **Leonardo D. Machado:** Writing – review & editing, Writing – original draft, Supervision, Resources, Project administration, Conceptualization.

Declaration of competing interest

The authors declare that they have no known competing financial interests or personal relationships that could have appeared to influence the work reported in this paper.

Acknowledgments

The authors thank the Brazilian Research Agencies CAPES, CNPq, and FAPESQ for their financial support. MB and LDM also acknowledge the support of the High Performance Computing Center at UFRN (NPAD/ UFRN). MLPJ acknowledges financial support from FAPDF (grant 00193-00001807/2023-16), CNPq (grant 444921/2024-9), and CAPES (grant 88887.005164/2024-00).

Appendix A. Supplementary data

Supplementary material related to this article can be found online at https://doi.org/10.1016/j.commatsci.2025.114087.

Data availability

Data will be made available on request.

References

[1] Y. Lei, T. Zhang, Y.-C. Lin, T. Granzier-Nakajima, G. Bepete, D.A. Kowalczyk, Z. Lin, D. Zhou, T.F. Schranghamer, A. Dodda, et al., Graphene and beyond: recent advances in two-dimensional materials synthesis, properties, and devices, ACS Nanosci. Au 2 (2022) 450–485.
[2] M. Xu, T. Liang, M. Shi, H. Chen, Graphene-like two-dimensional materials, Chem. Rev. 113 (2013) 3766–3798.
[3] S. Jana, A. Bandyopadhyay, S. Datta, D. Bhattacharya, D. Jana, Emerging properties of carbon based 2D material beyond graphene, J. Phys.: Condens. Matter. 34 (2021) 053001.
[4] J. Liu, H. Lu, Azugraphene: a new graphene-like hexagonal carbon allotrope with dirac cones, RSC Adv. 9 (2019) 34481–34485.
[5] Z. Zhang, H.D. Pham, D.F. Perepichka, R.Z. Khaliullin, Prediction of highly stable 2D carbon allotropes based on azulenoid kekulene, Nat. Commun. 15 (2024) 1953.
[6] A.G. Anderson Jr., B.M. Steckler, Azulene, A study of the visible absorption spectra and dipole moments of some 1-and 1 3-substituted azulenes, J. Am. Chem. Soc. 81 (1959) 4941–4946.
[7] J. Michl, E.W. Thulstrup, Why is azulene blue and anthracene white? a simple MO picture, Tetrahedron 32 (1976) 205–209.
[8] H. Xin, B. Hou, X. Gao, Azulene-based π-functional materials: design, synthesis, and applications, Acc. Chem. Res. 54 (2021) 1737–1753.
[9] E.C. Girão, A. Macmillan, V. Meunier, Classification of sp^2-bonded carbon allotropes in two dimensions, Carbon 203 (2023) 611–619.
[10] Y. Qi, M.A. Sadi, D. Hu, M. Zheng, Z. Wu, Y. Jiang, Y.P. Chen, Recent progress in strain engineering on van der waals 2D materials: Tunable electrical, electrochemical, magnetic, and optical properties, Adv. Mater. 35 (2023) 2205714.
[11] R.-X. Sun, Q.-Q. Guo, C.-F. Huo, X.-Q. Yan, Z.-B. Liu, J.-G. Tian, Critical strain-induced photoresponse in folded graphene superlattices, ACS Appl. Mater. Inter. 13 (2021) 21573–21581.
[12] R. Roldán, A. Castellanos-Gomez, E. Cappelluti, F. Guinea, Strain engineering in semiconducting two-dimensional crystals, J. Phys.: Condens. Matter. 27 (2015) 313201.
[13] R. Chegel, Strain tuning of optical and thermoelectric properties of monolayer BAs, Sci. Rep. 15 (2025) 1–13.
[14] S. Behzad, R. Chegel, Investigation of effects of interlayer interaction and biaxial strain on the phonon dispersion and dielectric response of hexagonal boron arsenide, Sci. Rep. 13 (2023) 21339.
[15] S. Behzad, R. Chegel, First-principles study of the band structure and optical spectra of germanium carbide under mechanical strain, J. Electron Spectrosc. 242 (2020) 146969.
[16] M.A. Bissett, M. Tsuji, H. Ago, Strain engineering the properties of graphene and other two-dimensional crystals, Phys. Chem. Chem. Phys. 16 (2014) 11124–11138.
[17] V.M. Pereira, A. Castro Neto, Strain engineering of graphene's electronic structure, Phys. Rev. Lett. 103 (2009) 046801.
[18] N. Peres, The electronic properties of graphene and its bilayer, Vacuum 83 (2009) 1248–1252.
[19] V.M. Pereira, A. Castro Neto, N. Peres, Tight-binding approach to uniaxial strain in graphene, Phys. Rev. B 80 (2009) 045401.
[20] S. Thomas, K. Ajith, S.U. Lee, M. Valsakumar, Assessment of the mechanical properties of monolayer graphene using the energy and strain-fluctuation methods, RSC Adv. 8 (2018) 27283–27292.
[21] G. Cocco, E. Cadelano, L. Colombo, Gap opening in graphene by shear strain, Phys. Rev. B 81 (2010) 241412.
[22] F. Zhang, S. Wu, S. Peng, Z. Sha, C.H. Wang, Synergism of binary carbon nanofibres and graphene nanoplates in improving sensitivity and stability of stretchable strain sensors, Compos. Sci. Technol. 172 (2019) 7–16.
[23] C. Mu, T. Zhu, Y. Zhou, Y. Gu, Q. Yang, B. Wu, In-situ growing of helical carbon fibers on graphene for high-performance flexible strain sensor, Colloids Surf. A 683 (2024) 132977.
[24] D. Sethy, K. Balasubramaniam, Graphene nano-platelet (GNP)–doped poly (methyl methacrylate)(PMMA) spray-coated piezoresistive-based 2D strain sensor under temperature environment on aluminium alloy 2024-T351, J. Nanopart. Res. 24 (2022) 118.
[25] L. Wei, Z. Wu, S. Tang, X. Qin, Y. Xiong, J. Li, E. Ruiz-Hitzky, X. Wang, Tracheid-inspired nanoarchitectured carbon-based aerogels with ultra-compressibility for wearable piezoresistive sensors, Carbon 203 (2023) 386–396.
[26] Y. Wang, L. Wang, T. Yang, X. Li, X. Zang, M. Zhu, K. Wang, D. Wu, H. Zhu, Wearable and highly sensitive graphene strain sensors for human motion monitoring, Adv. Funct. Mater. 24 (2014) 4666–4670.
[27] D. Akinwande, N. Petrone, J. Hone, Two-dimensional flexible nanoelectronics, Nat. Commun. 5 (2014) 5678.
[28] L. Gao, Flexible device applications of 2D semiconductors, Small 13 (2017) 1603994.
[29] Y.-T. Wu, T. Yan, Z.-J. Pan, Wearable carbon-based resistive sensors for strain detection: a review, IEEE Sens. J. 21 (2020) 4030–4043.
[30] S. Li, X. Xiao, J. Hu, M. Dong, Y. Zhang, R. Xu, X. Wang, J. Islam, Recent advances of carbon-based flexible strain sensors in physiological signal monitoring, ACS Appl. Electron. Mater. 2 (2020) 2282–2300.
[31] J.P. Perdew, K. Burke, M. Ernzerhof, Generalized gradient approximation made simple, Phys. Rev. Lett. 77 (1996) 3865.
[32] H.J. Monkhorst, J.D. Pack, Special points for Brillouin-zone integrations, Phys. Rev. B 13 (1976) 5188.
[33] X. Qin, H. Shang, H. Xiang, Z. Li, J. Yang, HONPAS: a linear scaling open-source solution for large system simulations, Int. J. Quantum Chem. 115 (2015) 647–655.
[34] A. Kokalj, XCrySDen–a new program for displaying crystalline structures and electron densities, J. Mol. Graph. Model. 17 (1999) 176–179.
[35] M. Bessa, S. Azevedo, A.C. Dias, L.D. Machado, Structural, electronic, and optical properties of inorganic and hybrid fullerene networks, Chem. Phys. Lett. 861 (2025) 141839.
[36] H.A. Kramers, La diffusion de la lumiere par les atomes, in: Atti Del Congresso Internazionale Dei Fisici, (Transactions of Volta Centenary Congress), Vol. 2, Como, 1927, pp. 545–557.
[37] R. De L. Kronig, On the theory of dispersion of X-rays, J. Opt. Soc. Am. 12 (1926) 547–557.
[38] D. da Silva, S. Azevedo, Optical properties of fluorinated boron nitride monolayers, Phys. E 134 (2021) 114899.

[39] L. Jiao, M. Hu, Y. Peng, Y. Luo, C. Li, Z. Chen, Electronic, elastic, and optical properties of monolayer BC_2N, J. Solid State Chem. 244 (2016) 120–128.
[40] J.P. Guedes, S. Azevedo, J.A. Gonçlves, S.E.L. Medeiros, J. Pontes, $B_xc_yn_z$ monolayers with full coverage of fluorine: A study of their structural, electronic and optical properties, Diam. Relat. Mater. (2023) 110146.
[41] D.G. Papageorgiou, I.A. Kinloch, R.J. Young, Mechanical properties of graphene and graphene-based nanocomposites, Prog. Mater. Sci. 90 (2017) 75–127.
[42] C. Lee, X. Wei, J.W. Kysar, J. Hone, Measurement of the elastic properties and intrinsic strength of monolayer graphene, Science 321 (2008) 385–388.